Article:

McGuire, C. and Rhodes, E.J. (2014) Determining fluvial sediment virtual velocity on the Mojave River using K-feldspar IRSL: Initial assessment. Quaternary International, 362. C. pp. 124-131. ISSN 1040-6182

https://doi.org/10.1016/j.quaint.2014.07.055

Determining fluvial sediment virtual velocity on the Mojave River using K-feldspar IRSL: Initial assessment

Christopher McGuire[1] & Edward J. Rhodes[1,2]

1 Earth, Planetary and Space Sciences, UCLA, Los Angeles, USA
2 Dept. of Geography, University of Sheffield, Sheffield, S10 2TN, UK

Author's accepted version of a paper published in Quaternary International 362, 124-131 (2015)
http://dx.doi.org/10.1016/j.quaint.2014.07.055

A b s t r a c t

The Mojave River of Southern California was chosen as a field site to investigate the applicability of luminescence dating to sediment transport rate problems. Grains in the active channel of the river are expected to show signs of partial bleaching and this makes it difficult to determine time since deposition accurately. A modification of the multiple elevated temperature post-IR IRSL (MET-pIRIR) procedure, (Buylaert et al., 2009; Li and Li, 2011), was used for K-feldspar grains (175-200 µm) at temperature increments of 50, 95, 140, 185, and 230 °C in order to provide more information about relative signal bleaching among samples. The measurements show an exponential decrease in equivalent dose (De) with distance down the Mojave River. Higher temperature pIRIR signals are bleached more slowly than lower temperature ones (Buylaert et al., 2009). The De for samples at 50 °C is roughly constant along the river. These results suggest cyclical bleaching and burial as grains are transported downriver and higher energy (deeper) traps are vacated. The pattern of De values for the Mojave River can be used to constrain the sediment transport rate for this river by building a model of growth and bleach for each temperature increment. A bleaching experiment was run with multiple aliquot samples for direct sunlight exposure times of 0, 10, 30, 300, 1000, 3000, 10,000, and 30,000 s. The MET-pIRIR procedure was applied at each temperature increment for each exposure time aliquot and the results for all exposure times were fit to the general order kinetics equation using a non-linear regression. The bleaching parameters were used in conjunction with the SAR growth curves to build a model of partial bleaching of grains during transport that is fitted with a c2 test to the pIRIR data from the Mojave River. This model is not a unique solution, but can be used to assess the likelihood of various sediment transport regimes.

Keywords:
Geomorphology
Infrared Stimulated Luminescence
Post IR-IRSL
Mojave River

1 Introduction

The rate of fine sand ($0.125 \text{ mm} < d < 0.250 \text{ mm}$) transport has been the subject of numerous theoretical studies and has implications for hillslope processes, denudation rates of mountain ranges, and basin analysis (Howard et al., 1994; Paola, 2000). Despite robust theory on the subject, there are few methods to measure fine sand fluvial transport in natural rivers (Milan and Large, 2014). Field studies of fine-sediment transport in streams and rivers primarily utilize tracer techniques (e.g., Crickmore, 1967). The tracer produces an above-background signal in individual sand grains that can be measured along a reach of a river as the sediment travels downstream. Individual grains with tracer are treated as a point mass using a centroid whose position over time can be converted into a virtual velocity (Milan and Large, 2014). Methods applied to larger sediment sizes, such as gravels and pebbles, include painting individual stones (Church and Hassan, 1992) and passive-integrated transponder (PIV) tags (Lamarre et al., 2005). Both of these methods are impractical for fine sand-sized particles, especially in large river systems. Methods that have been applied to fine sand include coating grains with fluorescent dyes (Rathburn and Kennedy, 1978) and enhancement of magnetic susceptibility of iron coatings on sand grains (Milan and Large, 2014). These methods have been successful in small rivers and streams, but application at the catchment scale or to large rivers would be time consuming and difficult to implement.

We propose to use natural luminescence of K-feldspar grains from samples along the Mojave River to estimate a virtual velocity of fine sediment transport. The geography of the Mojave River and the sample sites for this project are shown in Figure 1. Our method is not a "tracer method," as described above, because the process responsible for transporting the sediment (water flow) changes the luminescence signal we are measuring. Therefore, we create a simple forward model to explain how we expect the Infrared Stimulated Luminescence (IRSL) signal of fine sediment to change during water flow events. Future work will address the inverse problem of determining a virtual velocity for fine sediment in a more mathematically rigorous fashion.

Luminescence dating has proved a useful tool in geomorphology to date deposits of sediment and to understand the context of the events that created the deposits (e.g., Stokes, 1999; Rittenour, 2008). Prior research has shown that sensitivity of quartz grains changes in response to fluvial transport (Pietsch et al., 2008), and that quartz luminescence intensity changes in response to tributary inputs into large river systems (Stokes et al., 2001). We observe a roughly exponential decrease in multiple elevated temperature post-IR IRSL (MET-pIRIR) signals as a function of distance downriver, and propose that this result is a consequence of cycles of transport (signal bleaching) and deposition (signal growth) (Figure 2). This study explores how these preliminary results may be used to estimate sediment virtual velocity, defined as the distance travelled by the centroid of a group of individual grains (Figure 3) divided by the time interval between measurement locations (Milan and Large, 2014). We focus on the modern channel of the Mojave River as a case study and use a MET-pIRIR procedure (Buylaert et al., 2009; Li & Li, 2011; Fu & Li, 2013).

2 Regional Setting

The Mojave River in southern California is a terminal ephemeral stream that transports water and sediment through one of North America's driest regions (Enzel and Wells, 1997;

Enzel et al., 1992). The river flows from the San Bernardino Mountains, through the Mojave Desert towns of Victorville and Barstow and terminates at Silver Lake playa. Two upper streams, West Fork and Deep Creek, which are located on the north-facing slope of the San Bernardino Mountains, provide the majority of water flow for the entire river (Enzel and Wells, 1997). The confluence of the creeks is known as The Forks and the river flows from here to Silver Lake playa, a distance of about 200 km (Figure 1). The Forks receives an average of more than 1000 mm of precipitation per year (Enzel and Wells, 1997). However, the drainage basin overall is very dry; 90% of the watershed receives less than 150 mm/year (Enzel and Wells, 1997). At the Silver Lake terminus, 75 mm/year is the average (Enzel and Wells, 1997).

Hydrologic monitoring over the past century has shown that during normal or dry years water does not flow along the entire length of the river due to transmission loss and evaporation (Enzel and Wells, 1997). Significant flow, defined by Enzel and Wells (1997) as a peak discharge of >90 m^3s^{-1}, reaches Afton Canyon and Silver Lake only during extreme flood events (Enzel and Wells, 1997). The hydrologic record from USGS stream gages indicates that large floods on the Mojave River are correlated with the negative phase of the Northern Annular Mode (NAM^-) and Northern Pacific Gyre Oscillation (NPGO) southern displacement (Reheis et al., 2012). However, up until 1998, large magnitude floods also correlate with the positive (El Nino) phase of El Nino Southern Oscillation (ENSO) (Hereford et al., 2006). There is ambiguity associated with correlating multi-decadal time scale cycles using less than a century's worth of hydrologic data (Reheis et al., 2012). For the purposes of our model, the frequency of flooding on the Mojave River is an essential parameter; better constraints on this time interval would be useful, but are beyond the scope of this study.

3 Methods

3.1 Sample collection and preparation

Samples were collected from eight locations along the Mojave River (Figure 1). Sample locations were taken over a range of 156km, from the Forks to the Afton Canyon campsite. In several cases, long stretches of the river (i.e., >50 km) were inaccessible due to private property. Sample sites were selected in dry channel bar deposits, to ensure that the grains were last transported by water rather than wind. In order to reduce the recent effects of bioturbation, only samples with clear bedding structures were chosen. At each site, a hole was dug 0.3 to 0.5 m deep and an opaque 3-cm-diameter tube was pushed horizontally into the freshly cleaned wall of the hole. The tubes were capped and placed in a light protective bag. Location was recorded using a handheld GPS (GARMIN GPSmap78s). Samples were labeled according to the order of their collection. In the lab they were given numbers J0260-J0267 (Figure 1).

Samples were opened under controlled lighting conditions. The material from both ends of the tube was removed. The remaining material from the middle of the tube was separated by wet sieving into the desired grain size fractions. For mineralogical isolation, the grain size fraction 175-200 µm was chosen for each sample except J0263, for which the 200-250 µm sieve fraction was chosen due to lack of material in the desired size range. The samples were treated with HCl to remove carbonates. Density separation was performed using lithium metatungstate diluted to a density of 2.58 g/cm^3. For each sample, the denser material (mostly quartz) was frozen in a liquid nitrogen bath and the floating feldspar grains were poured off. The feldspar grains were washed and dried. No HF treatment was given due to the light color of the grains and bright signals observed in preliminary runs, indicating that grain coating was minimal. A monolayer of grains was glued to 1 cm diameter aluminum discs using viscous silicone oil. Three discs were made for each sample.

3.2 Luminescence measurements and MET-pIRIR procedure

Luminescence measurements were made using a Riso TA-DA-20D with blue-green filter combination (BG3 and BG39), for a transmission window of 340-470 nm. IRSL was measured using the MET-pIRIR procedure (Fu & Li, 2013). The MET-pIRIR procedure provides data from a series of thermally assisted IRSL measurements and was initially developed to find a stable, non-fading IRSL signal for K-feldspar (e.g., Li & Li, 2011). We make IRSL measurements at 50 ^{o}C, 95 ^{o}C, 140 ^{o}C, 185 ^{o}C, and 230 ^{o}C, with a pre-heat of 250 ^{o}C for 60 seconds. Our dose response curves were created using the SAR protocol (Murray & Wintle, 2000; Murray & Wintle, 2003). The measurement procedure is summarized in Table 1.

3.3 Bleaching experiment

In a separate experiment, we quantitatively describe how MET-pIRIR signals respond to sunlight exposure. The IRSL decay signal for feldspar has been described as a stretched-exponential (SE) function (Pagonis et al., 2012; Chen, 2003), and by the general order kinetics shown in Equation 1, below (Bailiff and Barnet, 1994; Poolton et al., 2009). Since we are interested only in the shape of IRSL decay in response to sunlight bleaching, the choice of one of the approximation functions listed above is somewhat arbitrary; although the parameters in these equations contain information about the underlying physical process of charge eviction from traps and recombination, they do so in an approximate way. We use the general order kinetics equation after Poolton et al. (2009) as a descriptive function, rather than an exact model, of IRSL intensity response to sunlight exposure.

The bleaching experiment measured pIRIR response to increasing sunlight exposure time and fit the data by varying the parameters of the general order kinetics equation:

$$I = \frac{I_0}{(1+at)^p} + R \qquad (1)$$

In Equation 1, parameter *a* is bleachability, *p* is order and *R* is residual. The parameter *a* represents capture cross section, light intensity, and initial trapped charge population (Poolton et al., 2009). The parameter *p* is known as the order of the reaction and contains information about how the reaction proceeds (McKeever, 1985). If *p* is 2, then Equation 1 is described as second order, indicating that luminescence emission is proportional to both trapped electron concentration and the number of unoccupied recombination sites, and that these quantities are exist in proportion of 1:1 (McKeever, 1985). In general order kinetics (i.e. $1 < p < 2$) luminescence displays neither first nor second order kinetic behavior (Bailiff and Barnet, 1994). We have modified the general order kinetics equation to include a residual term (*R* in Equation 1), which represents low intensity IRSL after long sunlight exposure time.

The sample from Barstow (JO265) was chosen as representative due to a lack of material from other sample sites. A total of 24 discs with 2-3 mm diameter monolayer grains were adhered (using silicon oil), to 1 cm diameter aluminum discs. In sets of three, the discs were exposed to direct sunlight at the University of California, Los Angeles for different amounts of time. The exposure times were 0, 10, 30, 300, 1000, 3000, 10000, 30000 seconds. Luminescence measurements were made using the MET-pIRIR procedure (see Table 1). The resulting data were fit to the general order kinetics equation using the Levenberg-Marquardt algorithm, subject to the constraint $1<p<2$ in Equation 1. If the algorithm is unconstrained, the solution for *p* for some pIRIR temperatures is less than 1, the physical meaning of which is not immediately clear. The bleaching experiment is subject to sensitivity changes and thermal transfer. Additionally, "anomalous stability," or the observation that the signal decays more slowly than expected by theory, may explain why the unconstrained solution for *p* is less than 1 (Chen et al., 2012). For the purposes of this simple model, we have decided to fit the bleach curves using the $1<p<2$ constraint, so that comparison among MET-pIRIR fits is more straightforward (see Section 4). The SAR dose response curves were fitted to an exponential function (Equation 2):

$$I = a\left(1 - exp(-(x + c)/b)\right) \qquad (2)$$

using Riso Analyst software (Levenberg-Marquart algorithm). Some of the dose response curves are actually exponential plus linear, but in order to reduce complexity of the model we chose to fit all curves with an exponential.

4 Results

In general, the equivalent dose of modern channel samples (J0262, J0263, J0267, J0266 and J0265) decreases downriver for each MET-pIRIR measurement (Figures 1, 2). The MET-pIRIR equivalent dose (D_e) from 230 $^{\circ}$C measurements decreases most slowly with distance downriver when compared with intermediate (185 $^{\circ}$C, 140 $^{\circ}$C and 95 $^{\circ}$C) MET-pIRIR D_e (Figure 2). The pIRSL signals are shown in Figure 2 with background subtracted, where background is defined as the last 50 channels in a 250 channel IRSL decay curve for a given sample. Although subsequent higher temperature pIRIR measurements are observed to decrease in an exponential shape down the river, the pIRIR measurements at 50°C decrease after the first sample site to a constant low level at the downriver sample sites. Laboratory experiments show that subsequent higher temperature assisted IRSL signals are bleached more slowly than lower temperature ones (Duller & Wintle, 1991; Buylaert et al., 2009; Li & Li, 2011).

A comparison of MET-pIRIR signals among a single sample site reveals that pIRIR D_e is proportional to IRSL measurement temperature, suggesting that each temperature increment in the MET-pIRIR removes an increasingly difficult to bleach IRSL signal (Figure 2). These pIRIR results are consistent with other workers' results (Fu and Li, 2013; Kars et al., *in press*). Furthermore, the results from our bleaching experiment can explain, to first order, the downriver trend of MET-pIRIR measurements as a consequence of different bleaching rates due to sunlight exposure during transport. Table 2 summarizes the results of the bleaching experiment for sample J0265 (Barstow) and fits are shown in Figure 4. The bleach curve for each MET-pIRIR temperature exhibits first order behavior (where *p* = 1 in Equation 1) when constrained to 1<p<2, except for IR_{50} that is between first and second order. One rationale for constraining *p* is to facilitate comparison of parameter *a* among different MET-pIRIR temperatures, as parameters *a* and *p* are not independent of each other in the general order kinetics equation. Parameter *a* for IR_{230} is about an order of magnitude lower than *a* for $IR_{50.}$ The unconstrained fit for IR_{230} is clearly better than the constrained fit by visual inspection of Figure 4e. However, in order to maintain continuity between each thermally assisted fit, we use the constrained results for *a* and *p* for IR_{230}.

The shape of each fitted bleach-curve is consistent with observations of modern channel sand samples in the Mojave River, suggesting that cyclical exposure to sunlight could explain the pattern (see Figures 2, 4). In Equation 1, parameter *a*, sometimes referred to as bleachability, decreases from pIRIR at 50 ^{o}C through subsequent MET-pIRIR measurements; our fitted results suggest that the bleachability parameter for pIRIR at 230 ^{o}C is an order of magnitude less than the bleachability for pIRIR at 50 ^{o}C.

We have removed three samples from the bleaching experiment and modeling due to two unrelated factors. Samples J0264 and J0261 were collected from a terrace deposit in a location where the main channel was inaccessible. These terrace samples have a higher equivalent dose than the modern channel upriver and downriver, as would be expected; since we do not model deposition and erosion of terraces explicitly, we have removed these results for the purposes of this simple model. The sample furthest from the headwaters is J0260, which was taken at Afton Canyon and was also removed, due to its higher pIRIR signal. A preliminary interpretation is that this sample has erosional inputs from nearby Tertiary to Quaternary alluvial-fan beds (Reheis and Redwine, 2008), which increases the average IRSL of small aliquot samples. For the purposes of this model, again we have elected to study the reach of the Mojave River from the headwaters to Barstow (Figure 1).

4.1 Model conceptual description

We construct a simple, first-order forward model of MET-pIRIR signal response to cycles of bleaching and growth, simulating how the luminescence characteristics of grains would respond to transport and deposition on the Mojave River. This forward model attempts to reproduce the MET-pIRIR data collected in the field by imagining a mass of sand in the Mojave River beginning at the headwaters (simulated time = 0), and travelling downriver from the headwaters (Sample J0262) to Barstow (Sample J0265) (Figure 1; Figure 3). The grains are assumed to come from bedrock with infinite age (signal at saturation) just upstream from our headwater sample site (Figure 1).

The model reproduces MET-pIRIR signals after a series of hypothetical floods, the frequency of which is roughly estimated to be 10 years. (We vary this parameter from 1 to 100 years in iterative runs of the model). The general order kinetics equation (Equation 1), using parameters shown in Table 2, represents bleaching during transport or deposition (if grains rest on the surface layer) and the dose response curve derived from Riso Analyst represents signal growth during burial (Figure 3). Specific steps in the algorithm for the model are shown in Appendix.

The pIRIR data from the Mojave River is fit to the model outputs using the assumption that each sample site in space represents a point in time for our hypothetical average sand travelling down the river. This forward model approximates "every flood," meaning that once the best fit is calculated, the number of floods between each data point times the interval between each flood is the amount of time it took for the samples to travel from one site to the next. We ignore the minor contribution of the time average sand grains spent in transport (on the order of days) since the total amount of time is dominated by deposition (on the order of years). We acknowledge that this method is heavily dependent on accurate flood frequency modeling, which is difficult to achieve at the resolution required. For this iteration of the forward model, we make major simplifying assumptions and evaluate model performance semi-quantitatively and graphically.

4.2 Model assumptions

Some key assumptions are necessary to simplify the model. We assume that the samples are representative of fluvial transport and that the MET-pIRIR measurements at each sample site would be repeatable if one were to directly observe the luminescence characteristics of a set of grains as it travelled the entire length of the river. Additionally, we assume weathering of feldspar grains does not contribute to changes in signal downriver. This is a potential problem given the time scales involved and either laboratory tests or statistical treatments should be implemented in a more advanced model to address this problem. We also assume that bleaching by attenuated light is analogous to a reduction in signal by direct sunlight. Recent work (Kars et al., *in press*) has shown that filtering of blue and ultraviolet light in water selectively affects the bleachability of higher temperature pIRIR signals. This observation was not accounted for in the present work. The period of bleaching time in the model is not representative of an actual amount of time that the sample has spent in the water column or on the surface of a channel bar. The model does not account for hydrologic transmission loss, which is known to occur on the Mojave River, even during large floods (Enzel and Wells, 1997). Transmission loss would decrease the frequency of transport events and increase burial time downriver, causing a relative increase in equivalent dose (in comparison with our model without transmission loss) with distance downriver. Finally, IRSL values are not corrected for anomalous fading.

4.3 Chi-squared minimization

The model calculates MET-pIRIR values for a bleach and growth pair (representing one transport, deposition and burial event) iteratively and checks how close each iteration output is to the observed Mojave River data using a χ^2 best fit. Since the distance between samples is known, the solution space within a critical χ^2 value provides upper and lower bounds on sediment virtual velocity for the river. The model implements a best fit to the data using Pearson's Chi Squared test, shown in Equation 3, modified after Davis (1973).

$$\chi^2 = min\left\{\frac{\left|IR_{model_{230}} - IR_{data_{230}}\right|^2}{IR_{230}} + \frac{\left|IR_{model_{185}} - IR_{data_{185}}\right|^2}{IR_{185}} + \frac{\left|IR_{model_{140}} - IR_{data_{140}}\right|^2}{IR_{140}} + \frac{\left|IR_{model_{95}} - IR_{data_{95}}\right|^2}{IR_{95}} + \frac{\left|IR_{model_{50}} - IR_{data_{50}}\right|^2}{IR_{50}}\right\} \quad (3)$$

A list of chi squared terms is calculated for each model generated point and the minimum is found simply by searching the list for the lowest value (for a description of the algorithm, see Appendix). A simulated time from the lowest chi squared model point is assigned to each sample location. The root mean square of all minimum chi squared is the output that is plotted on the χ^2 map (Figure 5). Robust error calculations were not carried out for this analysis (there is error on the bleach parameters for each signal and each dose response curve in addition to error in the natural IRSL intensity). The critical χ^2 value is 7.78, for 0.1 level of significance and four degrees of freedom. The results of the test are plotted as contour maps in a grid of the growth periods (flood intervals) and bleach times that we tested with the model, as shown in Figure 5. The range of plausible values for bleach time and growth period parameters is very large. Forward model results of time passed span three orders of magnitude, as discussed below.

5 Discussion

Model runs that are within the χ^2 tolerance can be forward modelled, which graphically outputs model generated points for comparison with measured data points (Figure 6). The forward model is in the space of IRSL signal as a function of simulated time in years, where t = 0 is a hypothetical sample at the first sampling location (Figure 3, Figure 6). This allows us to solve for the amount of simulated time passed between the headwaters sample J0262 and samples downriver (see Figure 1). The least amount of simulated time output by the model is 20 years and the maximum amount of time passed is 7500 years.

The time interval range is too large to describe sediment virtual velocity. However, we can use other information to help constrain the problem further. Based on hydrologic data over the last century, the Mojave River flows continuously from the headwaters to Barstow (sample J0265, Figure 1) roughly once every decade (Enzel and Wells, 1997), although individual examples of recurrence interval vary widely from 1 year to 12 years as measured by USGS stream gage monitoring (USGS National Water Information System, see references). If we assume that the flood frequency (and thus the growth period) has remained constant, we can solve the least χ^2 for the bleach time parameter only. The solution space ranges from 1 to 8 seconds of cyclical bleaching and the results are shown in the inset of Figure 5. In the forward model, time passed from the headwaters to Barstow ranges from 210 to 800 years. Figure 6 shows that the forward model only accurately models pIRIR 230°C for the entire length of the river. This could be a result of not taking river flow transmission loss into account. Less frequent water flow as a function of distance from the headwaters would increase the recurrence interval and reduce the magnitude of transport events, thereby limiting the light exposure of buried grains. The model presented in this paper overestimates how much light downriver samples receive relative to samples further upriver. Another possibility is that only the largest floods are responsible for channel deposits and that the frequency and magnitude of bleaching is far more heterogeneous than this model represents. In general, a more advanced model and more measurements are necessary to improve the accuracy of the least χ^2 forward model method.

Our preliminary results suggest that flow is frequent enough that the IRSL signals decrease downriver, overcoming signal growth during burial time, from the headwaters to at least Barstow. The result at Afton Canyon, although somewhat ambiguous, may represent a rise in equivalent dose due to less frequent transport. Greater sampling density, and a model with robust hydrologic inputs is needed to resolve this problem.

The MET-pIRIR laboratory methods developed in previous studies can be applied to determine a range of possible transport times for sediment in the modern channel of the Mojave River. A larger data set should provide better constraints on our estimates and allow for robust statistical analysis of variability. The growth period parameter is likely to remain insensitive to constraint because change in signal due to growth occurs on a time scale that is approximately 5 orders of magnitude greater than change in signal due to bleaching. A more constructive approach may be to solve for the bleach time parameter only while using a distribution of growth periods with a mean based on prior hydrologic data from the region. In either case, additional sampling should improve the accuracy of the solution.

6 Conclusion

The MET-pIRIR measurement process used in conjunction with a model for environmental changes in luminescence, such as that presented here, has the potential to become a powerful new tool to assess source to sink processes. The applicability of this approach to fluvial systems other than the Mojave River may be wide-reaching. Other authors have noted exponential decrease in equivalent dose (or "effective dose" since the dose does not represent the age of the deposit) for small aliquot quartz samples with distance from source in large drainage systems (e.g., Stokes et al., 2001). However, the MET-pIRIR procedure may provide richer data with which to distinguish components of sunlight bleaching, making K-feldspar the preferable mineral to determine virtual velocities or sediment residence times in fluvial systems.

Appendix

Description of Forward Model Algorithm Steps

1. Initial simulated point is IR_{230} at saturation in IRSL units (for all following iterations, IRSL is from step 6)
2. IRSL value from step 1 is bleached for t_b seconds using general order kinetics equation (Equation 1, see text) with IR_{230} parameters determined by experiment.
3. New IRSL value after step 2 is converted to equivalent dose units using SAR growth curve (Murray and Wintle, 2003), which has been rearranged from Equation 2 (see text):

$$x = -c - b\left(\ln(1 - I/a)\right)$$

4. Growth period (in D_e units) is added to equivalent dose value determined in step 3.
5. New D_e after growth is converted to IRSL units using Equation 2 in its usual form.
6. The corresponding time in Equation 1 for the IRSL value from step 5 (x-axis value on a IRSL decay curve) is found by rearranging Equation 1

$$t = \frac{\left(\sqrt[p]{\left({I_0}/{I} - R\right)} - 1\right)}{a}$$

7. This time is added to t_b in step 2 and we repeat steps 2 through 7 for 225 iterations (The number of iterations was determined by running the entire algorithm several times until the fastest, in total simulated time, convergence was reached.)
8. Repeat steps 1 through 7 for IR_{185}, IR_{140}, IR_{95} and $IR_{50.}$
9. Create a list with 225 repetitions of each MET-pIRIR measurement at each Mojave River sample location.
10. Insert each list into the corresponding temperature data term in Equation 3 (i.e. $\boldsymbol{IR_{data_{230}}}$ for the IR_{230} data at each sample location).

$$\boldsymbol{\chi^2 = min\left\{\frac{\left|IR_{model_{230}} - IR_{data_{230}}\right|^2}{IR_{230}} + \frac{\left|IR_{model_{185}} - IR_{data_{185}}\right|^2}{IR_{185}} + \frac{\left|IR_{model_{140}} - IR_{data_{140}}\right|^2}{IR_{140}} + \frac{\left|IR_{model_{95}} - IR_{data_{95}}\right|^2}{IR_{95}} + \frac{\left|IR_{model_{50}} - IR_{data_{50}}\right|^2}{IR_{50}}\right\}}$$

11. Search every resulting chi squared value for the lowest one.
12. Repeat 10,000 times in order to test 100 different bleach time inputs and 100 different growth period inputs.

Acknowledgements

We would like to thank Utah State University for hosting the 9th New World Luminescence Dating Workshop as it allowed us the opportunity to present our ideas and receive feedback that resulted in this manuscript. We thank Marith Reheis and an anonymous reviewer for their careful revisions of this manuscript, which greatly improved the content of the document. Conversations with Amanda Keen-Zebert provided helpful guidance about sediment transport terminology. We also thank Dallon Stang for help preparing samples in the laboratory.

References

Bailiff, I.K. and Barnett, S. M., 1994. Characteristics of infrared stimulated luminescence from a feldspar at low temperatures. Radiation Measurements, 23: 541-546.

Buylaert, J. P., Murray, A. S., Thomsen, K. J., and Jain, M., 2009. Testing the potential of an elevated temperature IRSL signal from K-feldspar. Radiation Measurements, 44: 560-565.

Chen, R., 2003. Apparent stretched-exponential luminescence decay in crystalline solids. Journal of Luminescence, 102-103. 510-518.

Chen, R., Lawless, J. L., Pagonia, V., 2012. Two-stage thermal stimulation of thermoluminescence. Radiation Measurements, 47: 809-813.

Church, M., Hassan, M. A., 1992. Size and distance of travel of unconstrained clasts on a streambed. Water Resources Research, 28: 299 -303.

Crickmore, M. J., 1967. Measurement of sand transport in rivers with special reference to tracer methods. Sedimentology, 8: 175 – 228.

Davis, John C., 1973. Statistics and Data Analysis in Geology. John Wiley and Sons, New York.

Duller, G. A. T. & Wintle, A., 1991. On infrared stimulated luminescence at elevated temperatures. International Journal of Radiation Applications and Instrumentation, 18: 379 – 384.

Enzel, Y. Brown, W. J., Anderson, R. Y., McFadden, L. D., Wells, S. G., 1992. Short-duration Holocene lakes in the Mojave River drainage basin, southern California. Quaternary Research, 38: 60-73.

Enzel, Y. and Wells, S. G., 1997. Extracting Holocene paleohydrology and paleoclimatology information from modern extreme flood events: an example from southern California. Geomorphology, 19: 203-226.

Fu, X., Li, S., 2013. A modified multi-elevated temperature post IR-IRSL protocol for dating Holocene sediments using K-feldspar. Quaternary Geochronology, 17: 44-54.

Gesch, D.B., 2007, The National Elevation Dataset, in Maune, D., ed., Digital Elevation Model Technologies and Applications: The DEM Users Manual, 2nd Edition: Bethesda, Maryland, American Society for Photogrammetry and Remote Sensing, pp 99-118.

Gesch, D., Oimoen, M., Greenlee, S., Nelson, C., Steuck, M., and Tyler, D., 2002, The National Elevation Dataset: Photogrammetric Engineering and Remote Sensing, 68: 5-11.

Hereford, R., Webb, R. H., Longpre, C. I., 2006. Precipitation history and ecosystem responds to multidecadal precipitation variability in the Mojave Desert region, 1893 - 2001. Journal of Arid Environments, 67: 13 - 34.

Howard, A. D., Dietrich, W. E., Deidl, M. A., 1994. Modeling fluvial erosion on regional to continental scales. Journal of Geophysical Research, 99: 13971 - 13986.

Kars, R. H., Reimann, T., Ankjaergaard, C., Wallinga, J., *in press*. Bleaching of the post-IR IRSL signal: new insights for feldspar luminescence dating. Boreas, doi: 10.1111/bor.12082

Lamarre, H., MacVicar, B., Roy, A. G., 2005. Using passive integrated transponder (PIT) tags to investigate sediment transport in gravel-bed rivers. Journal of Sedimentary Research, 75: 736 – 741.

Li, B., Li, S., 2011. Luminescence dating of K-feldspar from sediments: A protocol without anomalous fading correction. Quaternary Geochronology, 6: 469-479.

Milan, D. J., Large, A. R. G., 2014. Magnetic tracing of fine-sediment over pool-riffle morphology. Catena, 115: 134 – 149.

McKeever, S. W. S., 1985. Thermoluminescence of solids. Cambridge University Press, Cambridge.

Murray, A. S., Wintle, A. G., 2000. Luminescence dating of quartz using an improved single-aliquot regenerative-dose protocol. Radiation Measurements, 32: 57-73.

Murray, A. S., Wintle, A. G., 2003. The single aliquot regenerative dose protocol: potential for improvements in reliability. Radiation Measurements, 37: 337-381.

Pagonis, V., Marthekai, P., Singhvi, A. K., Thomas, J., Balaram, V., Kitis, G., Chen, R., 2012. Time-resolved infrared stimulated luminescence signals in feldspars: Analysis based on exponential and stretched exponential functions. Journal of Luminescence, 132: 2330-2340.

Paola, C., 2000. Quantitative models of sedimentary basin filling. Sedimentology, 47: 121 - 178.

Pietsch, T. J., Olley, J. M., Nanson, G. C., 2008, Fluvial transport as a natural luminescence sensitizer of quartz. Quaternary Geochronology, 3: 365 – 376.

Poolton, N. R. J., Kars, R. H., Wallinga, J., Bos, A. J. J., 2009. Direct evidence for the participation of band-tails and excited-state tunneling in the luminescence of irradiated feldspars. Journal of Physics: Condensed Matter, 21: doi: 10.1088/0953-8984/21/48/485505.

Rathburn, R. E., Kennedy, V. C., 1978. Transport and dispersion of fluorescent tracer particles for the dune-bed condition, Atrisco Feeder canal near Bernalillo, New Mexico. USGS Professional Paper: 1037.

Reheis, M. C., Bright, J., Lund, S. P., Miller, D.M., Skipp, G., Fleck, R. J., 2012. A half-million-year record of paleoclimate from the Lake Manix Core, Mojave Desert, California. Palaeogeography, Palaeoclimatology, Palaeoecology, 365: 11 - 37.

Reheis, M. C., Redwine, J. L., 2008. Lake Manix shorelines and Afton Canyon terraces: Implications for incision of Afton Canyon. Reheis, M.C., Hershler, R., and Miller, D.M., eds., in Late Cenozoic Drainage History of the Southwestern Great Basin and Lower Colorado River Region: Geologic and Biotic Perspectives: Geologic Society of America, Special Paper 349, pp 227 – 259.

Rittenour, T., 2008. Luminescence dating of fluvial deposits: applications to geomorphic, paleoseismic and archeological research. Special Issue, Boreas, 37: 613-635.

Stokes, S., Bray, H.E., Blum, M.D., 2001. Optical resetting in large drainage basins: tests of zeroing assumptions using single-aliquot procedures. Quaternary Science Reviews, 20: 879-885.

Stokes, S., 1999. Luminescence dating applications in geomorphological research. Geomorphology, 29: 153-171.

USGS National Water Information System, http://waterdata.usgs.gov/ca/nwis/uv?site_no=10262500 (accessed July 3, 2014).

Figure Captions

Figure 1: Map of field site: Samples from the Mojave River are marked with a triangle and their respective laboratory codes. All samples are from point bar or channel bar structures that have been preserved since deposition, with the exception of samples J0261 and J0264. These samples were taken from a terrace in a location where the river was inaccessible. They are excluded from the present study for this reason. Sample J0260 is also excluded, see text for discussion. Topographic data from USGS National Elevation Dataset (http://ned.usgs.gov; Gesch et al., 2002; Gesch, 2007).

Figure 2: Equivalent dose decreases with distance from the furthest upstream sample, J0262 (Figure 1). The subsequent higher MET-pIRIR measurements bleach more slowly than lower temperature ones. Equivalent dose for IR_{50} remains at a constant low level after the first sample site.

Figure 3: Conceptual model of bleaching and growth differences for IR_{50} and IR_{230}. Bleaching varies significantly, while growth of the signal is similar. This allows for the signal response to sunlight exposure in the environment to be measurably different. Note that the simulated time scale for bleaching is greatly exaggerated in this figure. The upper half of the diagram represents IRSL field measurements and the trends observed downriver. The sand patches indicate an average mass of sand (centroid shown with black dot), the IRSL characteristics of which are assumed to be represented by the sample discs. The lower half shows a mapping of IRSL values to simulated time of the forward model. Since the number of flood events between

each location is unknown, the change in simulated time (Δt*) is determined by the best fit of field measurements to model outputs. The unknown amount of growth between deposition and collection of the sample contributes to uncertainty in Δt*.

Figure 4: Bleaching experiment data fitted to the general order kinetics equation (Equation 2) for each temperature assisted met-pIRIR measurement. Fits are shown with residuals below. (a) IR_{50} (b) IR_{95} (c) IR_{140} (d) IR_{185} (e) IR_{230} fit with constraint $1<p<2$ and IR_{230} without constraint, see section 4.

Figure 5: Model χ^2 test results. The contours represent values of χ^2 test statistic for 100 bleach time inputs and 1000 growth period inputs. For a 0.1 level of significance and four degrees of freedom, the critical χ^2 value is 7.78, meaning that any model with input parameters falling within this contour is accepted as consistent with the data. The inset shows the χ^2 for 10 year growth periods (decadal) and the interval of (1,100) bleach times. The dashed line indicates the 0.1 significance level, below which lie acceptable model fits.

Figure 6: Forward Model. This output is for an input growth period of 10 years and an input bleach time of 7 seconds. The resulting total simulated time is 270 years. IR_{230} fits well, but lower temperature pIRIR measurements fit less well due to decay of model to background level, see text for discussion.

Table Captions

Table 1: The MET-pIRIR protocol used in this study, after Fu and Li, 2013.
Table 2: The results for fitted parameters of Equation 1 for each MET-pIRIR. Parameter a has units of s^{-1}, p is unitless and R is arbitrary units of IRSL intensity.

Table 1

Step	Measurement
1	Natural, Regenerative Dose
2	Preheat 250^{o}C, 60s
3	IR diodes at 50^{o}C
4	IR diodes at 95^{o}C
5	IR diodes at 140^{o}C
6	IR diodes at 185^{o}C
7	IR diodes at 230^{o}C
8	Test Dose
9	Preheat 250^{o}C, 60s
10	IR diodes at 50^{o}C
11	IR diodes at 95^{o}C
12	IR diodes at 140^{o}C
13	IR diodes at 185^{o}C
14	IR diodes at 230^{o}C
15	Hot bleach IR diodes at 290^{o}C, 40s
Repeat from step 1	

Table 2

IR Stimulation	a	p	R
IR_{50}	0.074	1.6178	0.0439
IR_{95}	0.0526	1	0.0476
IR_{140}	0.0292	1	0.1409
IR_{185}	0.0169	1	0.2513
IR_{230}	0.0064	1	0.2903

Figure 1

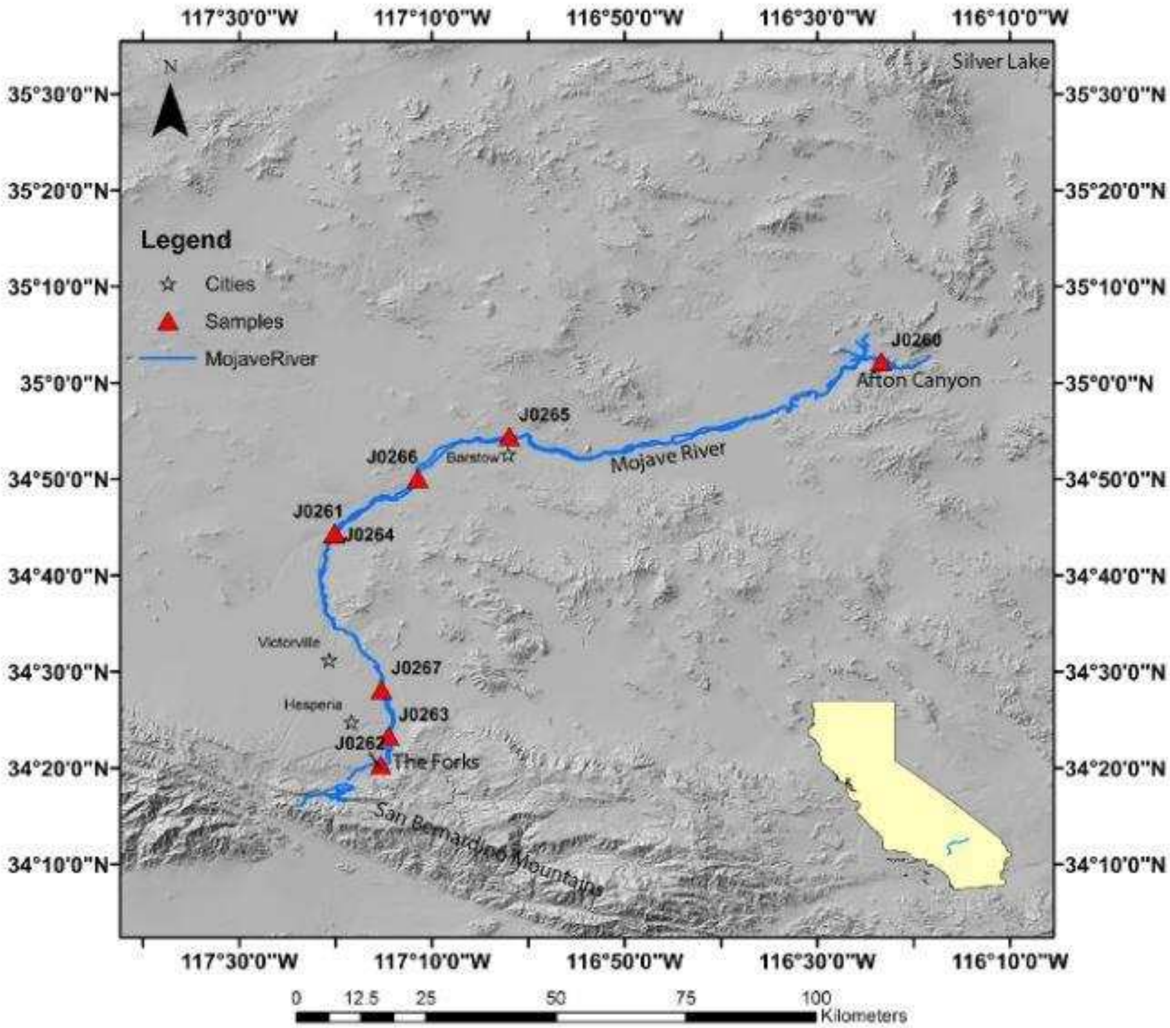
117°30'0"W
117°10'0"W
116°50'0"W
116°30'0"W
116°10'0"W
35°30'0"N
35°20'0"N
35°10'0"N
35°0'0"N
34°50'0"N
34°40'0"N
34°30'0"N
34°20'0"N
34°10'0"N
N
Silver Lake
Legend
Cities
Samples
MojaveRiver
J0260
Afton Canyon
J0265
Barstow
Mojave River
J0266
J0261
J0264
Victorville
J0267
Hesperia
J0263
J0262
The Forks
San Bernardino Mountains
0
12.5
25
50
75
100
Kilometers

Figure 2

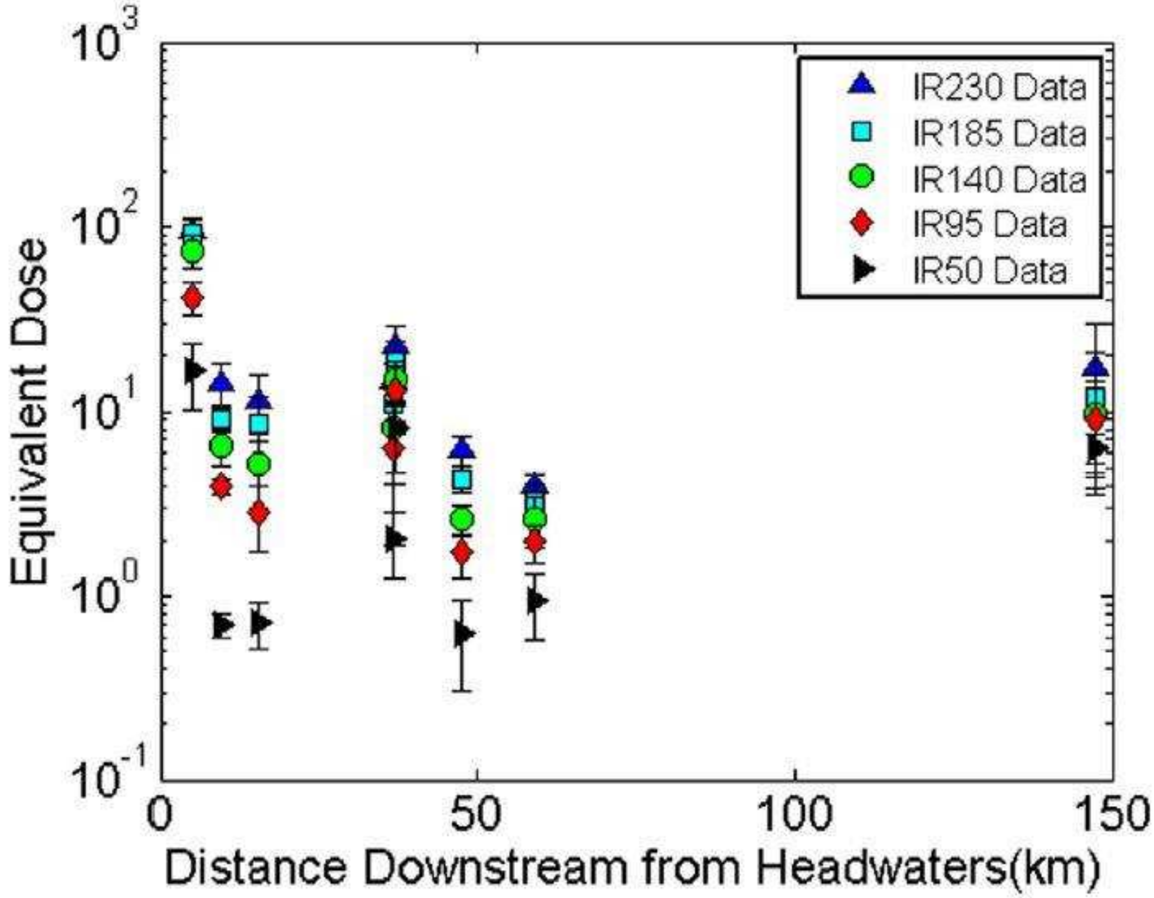

IR230 Data
IR185 Data
IR140 Data
IR95 Data
IR50 Data
Equivalent Dose
Distance Downstream from Headwaters(km)

583 Figure 3

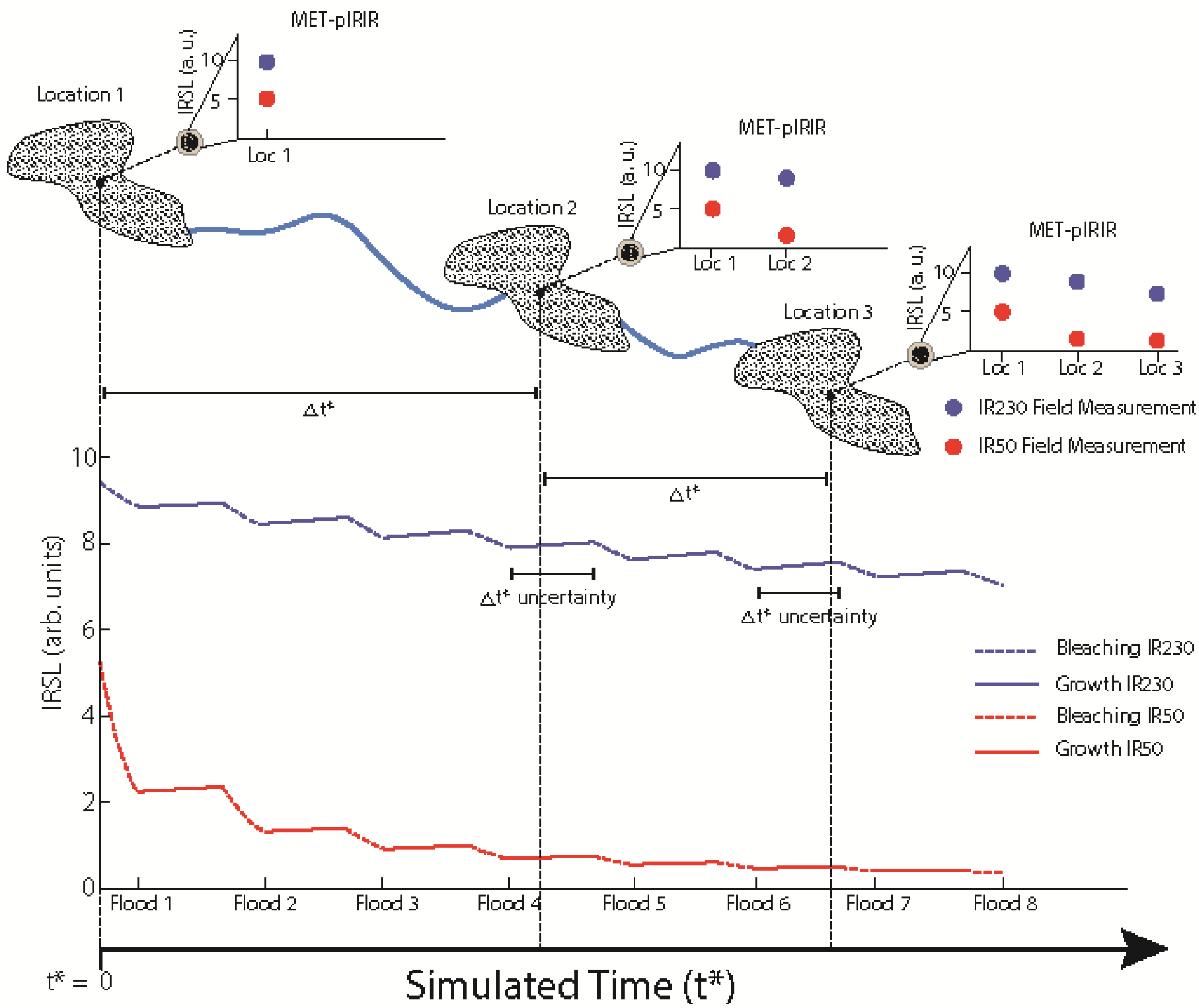

584
585

Figure 4 a-d

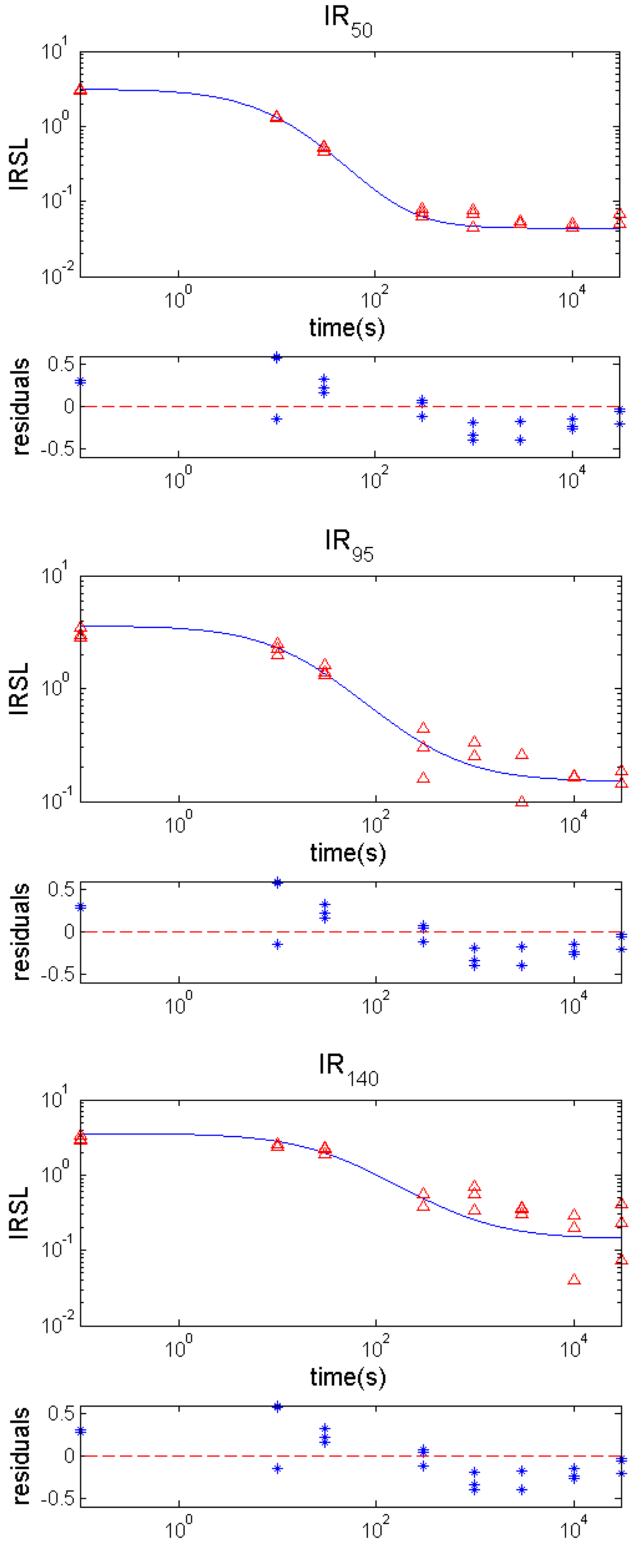

IR50
IRSL
time(s)
residuals
IR95
IRSL
time(s)
residuals
IR140
IRSL
time(s)
residuals

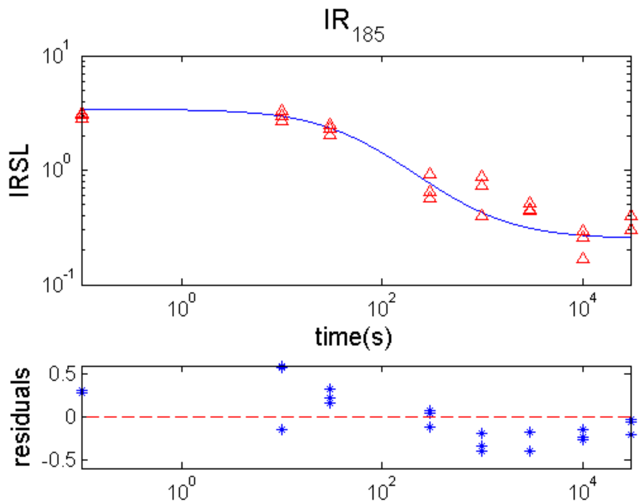

IR185
IRSL
time(s)
residuals

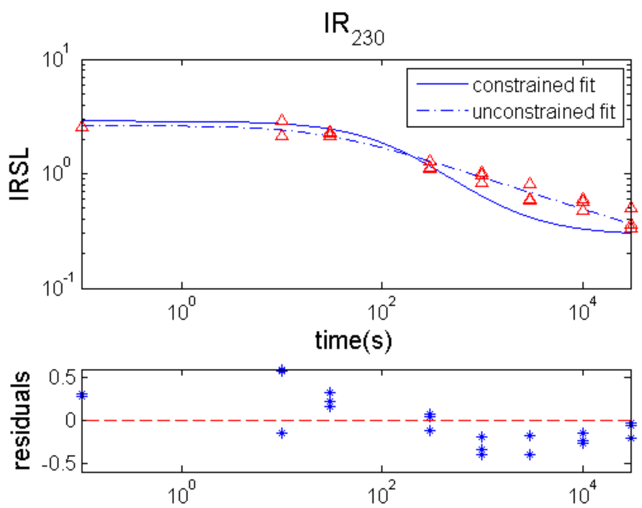

IR230
constrained fit
unconstrained fit
IRSL
time(s)
residuals

593 <u>Figure 5</u>

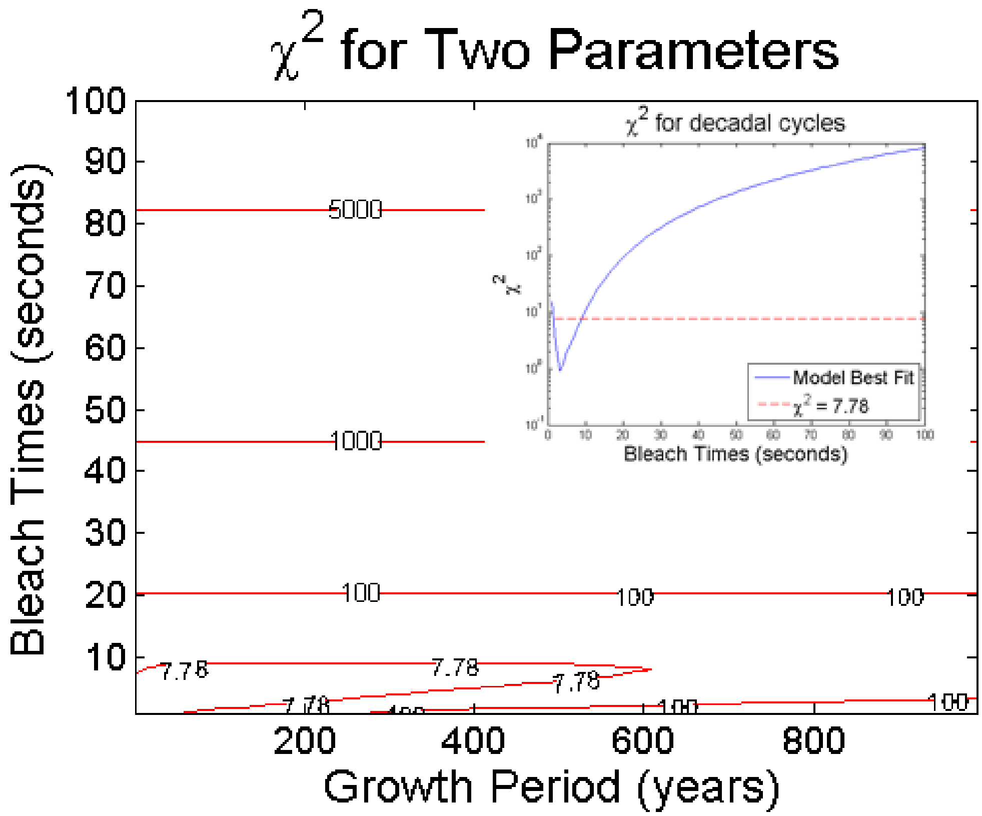

594

595

Figure 6

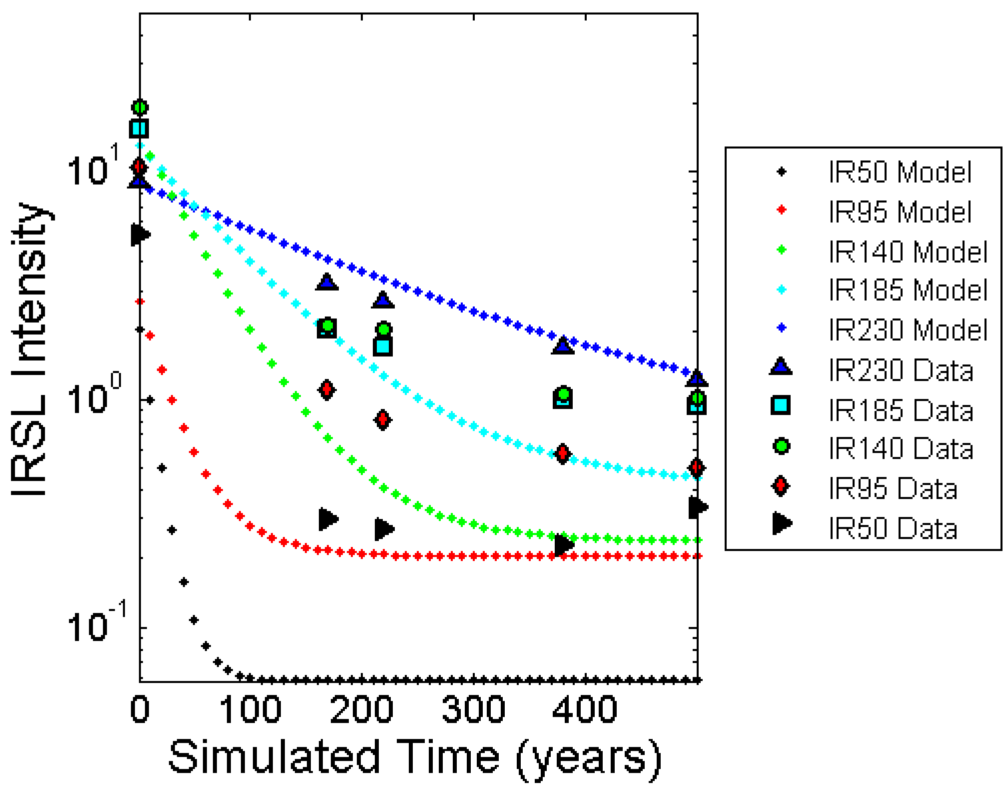
IRSL Intensity
10^{1}
10^{0}
10^{-1}
0
100
200
300
400
Simulated Time (years)
IR50 Model
IR95 Model
IR140 Model
IR185 Model
IR230 Model
IR230 Data
IR185 Data
IR140 Data
IR95 Data
IR50 Data